Gigawatt-Level Microwave Bursts from a New Type of Virtual-Cathode Oscillator

H. A. Davis, R. R. Bartsch, T. J. T. Kwan, E. G. Sherwood, and R. M. Stringfield
Los Alamos National Laboratory, Los Alamos, New Mexico 87545
(Received 13 February 1987)

We describe experiments that demonstrate a new method for producing high-power microwave emission. The unstable oscillations of a virtual cathode, which forms when a magnetized relativistic electron beam is injected into a circular waveguide, generate the microwave radiation. In contrast to previous virtual-cathode microwave-generation techniques, electrons in the waveguide cannot be reflected back into the diode. Using this technique, we have produced 1.4 GW at 3.9 GHz with several hundred megawatts radiated in harmonic radiation.

PACS numbers: 52.60.+h, 52.65.+z, 85.10.Ka

Much progress has been made recently with use of intense relativistic electron beams (with currents from 1 to 200 kA, and energies from 0.1 to 10 MeV) for the generation of ultrahigh-power microwave pulses.[1] Various techniques have yielded output power levels up to several gigawatts having frequencies of 1–100 GHz and pulse durations from 1.0 to 500 ns. Devices that exploit virtual cathodes, which form when an electron beam above the space-charge–limiting current is injected into a drift space, are among the most promising sources.[2–11] The virtual cathode is an unstable region of negative potential which reflects some of the electrons back into the source region. These sources have many advantages over more conventional microwave devices, including current levels above the space-charge limit, no need for an interaction structure (this may allow higher breakdown levels), simplicity of the hardware configuration, and potential for high-frequency operation.

Two models have been proposed to explain the microwave generation by virtual cathodes. In the first,[2] electrons being reflected between the real and virtual cathodes bunch in phase in the presence of an oscillatory electric field. The electrons lose energy to the radiation field, thus producing microwave emission. The microwave frequency is approximately the electron bounce frequency between the real and virtual cathodes. In the second model,[6] longitudinal oscillations of the virtual cathode excite axisymmetric-transverse-magnetic waveguide modes. One-dimensional calculations show that the radiation frequency scales with the relativistic beam plasma frequency given by

$$f_p = (n_e e^2/\pi\gamma m)^{1/2},$$

where f_p is in hertz, n_e is the injected beam density (in electrons/cm^3), e and m are the electron charge and mass, respectively (in cgs units), and γ is the Lorentz factor. As the injected current increases from one to several times the space-charge–limiting current, the radiation frequency increases from 1 to $(2\pi)^{1/2}$ times f_p.

Computer calculations show that both processes are present, although one usually prevails. The competition between these mechanisms leads to incoherent, multimode, and inefficient microwave output. One solution to this problem is to arrange the experimental geometry so the two processes have nearly the same frequency.[10] Computer modeling then shows frequency locking and some improvement in efficiency. Another approach, demonstrated experimentally here for the first time, is to eliminate the electron being reflected altogether.[6,12,13]

Our technique, shown in Fig. 1, is to inject an intense electron beam into a circular waveguide through a slot in a range-thick anode. An axial magnetic field guides the electrons through the slot. The injected beam current is above the space-charge limit in the circular waveguide given by the relation

$$I = 8.5(\gamma^{2/3} - 1)^{3/2}/\ln(b/a),$$

where I is the limiting current in kiloamperes, b is the waveguide radius, a is the beam radius, and γ is the Lorentz factor. This leads to formation of a virtual cathode downstream of the anode. The fields of the virtual cathode impart transverse momentum to the reflected electrons such that the anode intercepts a large fraction of them and prevents them from reentering the diode region. Also, if the applied magnetic field is weak enough, the radial forces acting on the beam do not balance,[14] and the beam radius can increase in the region downstream of the anode. This causes the reflected electrons to strike the anode outside the slow outer radius.

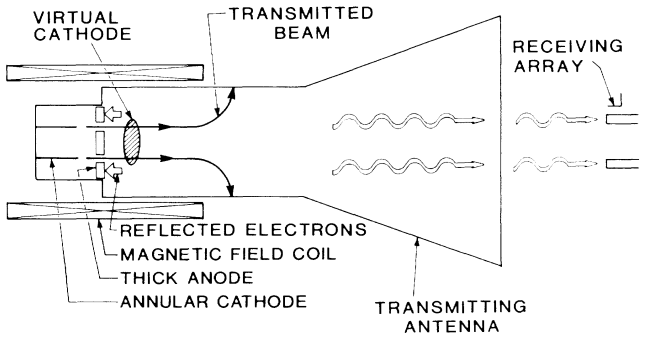

FIG. 1. The experimental arrangement. The axial dimension has been compressed.

© 1987 The American Physical Society

In both cases, electrons that turn around are prevented from reentering the diode. This minimizes interpenetration of the incoming and reflected electron flows, a condition that severely increases the divergence and energy spread of the incoming beam through streaming instabilities. Further, the competing reflected mode of radiation production is eliminated.

Computer calculations have shown that this approach potentially leads to enhanced efficiency, more monochromatic output, and better mode control than conventional unmagnetized or magnetized systems.[13] These calculations predict efficiencies of 15%–20% with bandwidths of less than a few percent, in some cases. More conventional virtual-cathode devices produce 0%–3% efficiency and 10% bandwidth. An additional benefit is that the thick anodes survive firing at current densities that destroy the usual thin anode foils. This enables repetitive operation without the replacement of the anode between shots. We demonstrate below that inhibition of the electron being reflected into the diode region has been achieved and report very high microwave power levels. We make comparisons with computer modeling to delineate the various physical phenomena. In these preliminary experiments, we have not yet demonstrated enhanced radiation efficiency, and limitations in diagnostic resolution have not allowed predictions of improved bandwidth and modal purity to be checked. These issues will be studied in more optimized future experiments with improved diagnostics.

The beam electrons were emitted from a 6-cm-diam annular cathode having a 0.05-cm wall thickness. The cathode was centered inside an 11.4-cm-diam housing and was spaced 1 to 3.7 cm from the anode face. The anode was 1-cm-thick, high-density graphite with a 0.5-cm-wide azimuthal slot centered on a 6-cm diameter. The center of the anode was supported by three radial spokes that intercepted approximately 6% of the beam current. The beam was injected through the slot into an 18-cm-diam circular waveguide, and the entire diode and the first 16 cm of the waveguide were immersed in a uniform axial magnetic field variable from 0 to 30 kG. The microwave radiation produced downstream of the anode foil propagated along 1.25 m of circular waveguide. A 1.25-m-long conical antenna, terminated by a 0.6-m-diam vacuum window large enough to avoid microwave breakdown at the vacuum-air interface, followed the waveguide. The diode region and output waveguide base pressure were approximately 3×10^{-5} Torr.

We sampled the radiation field in a plane 2 m from the output window with open sections of standard rectangular waveguide. These signals were transmitted through short runs of waveguide to heavily attenuated, fast-response-time detectors (1-ns system rise time) outside the hard x-ray field of the electron beam. Frequency coverage was from 2 to 40 GHz. In the frequency bands from 8 to 40 GHz, signals were transmitted to detectors through a second set of much longer runs of waveguide to disperse the signals for frequency identification. In the frequency bands from 4 to 8 GHz, phase comparison between signals transmitted through different length cables was used to make frequency measurements. Below 4 GHz, bandpass filter and waveguide dispersion techniques were used. We inferred power levels by integrating radial profiles measured by scanning the radiation field from shot to shot. Mode identification was made from the profile data and observation of the light output from an array of fluorescent tubes illuminated by microwaves.

As the anode-to-cathode gap was varied from 1.7 to 3.7 cm, the diode voltage, diode current, and propagated current varied from 1.4 to 1.9 MeV, 48 to 35 kA, and 14 to 20 kA, respectively. Figure 2 shows typical diode current, propagated beam current, and microwave envelope signals for an applied magnetic field of 9.3 kG and anode-cathode gap of 3.7 cm. This configuration, which produced strong microwave output, will be referred to as the standard case in the following. The peak diode current, peak propagated current, and beam pulse width (full width at half maximum) are 35 kA, 18 kA, and 70 ns, respectively. The diode voltage waveform follows the diode current quite closely and has a peak of 1.9 MV. The microwave burst is about 45 ns in duration

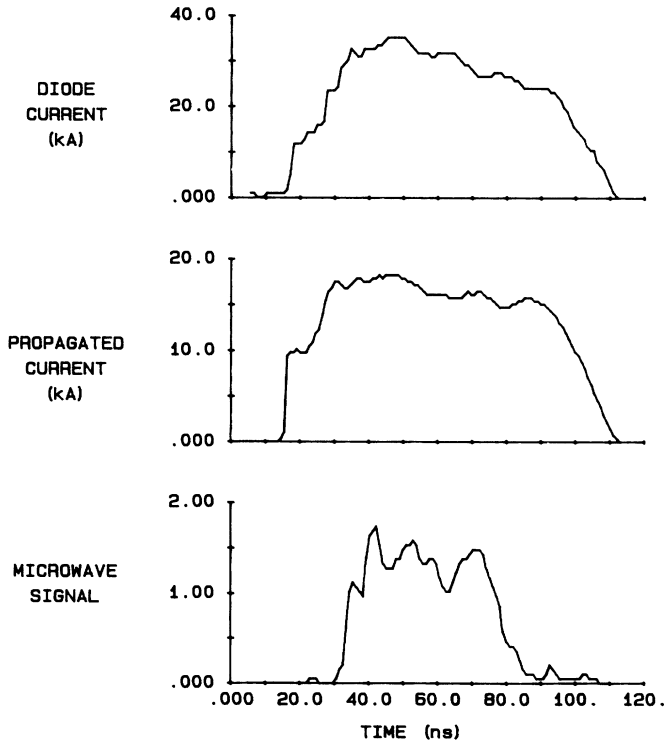

FIG. 2. Diode current, transmitted beam current, and microwave envelope (relative vertical scale) for $B=9.3$ kG and 3.7-cm anode-cathode gap.

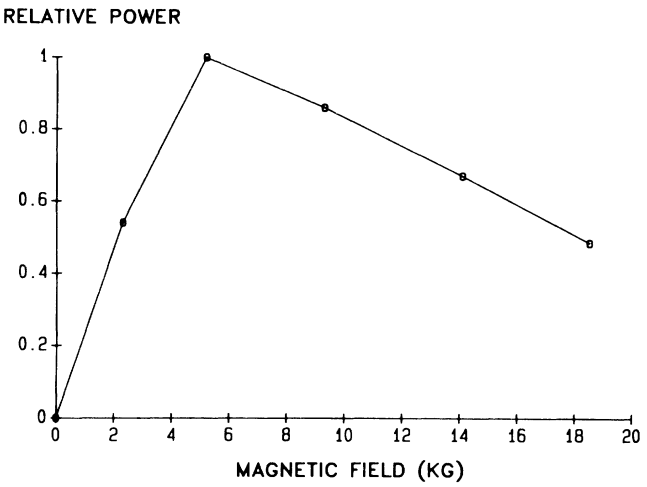

FIG. 3. Relative microwave power vs applied magnetic field for an anode-cathode gap of 2.6 cm.

(half-power points).

The goal of initial experiments was to establish that the electron being reflected into the diode region could be suppressed as predicted. First, we measured the power as a function of magnetic field strength. Figure 3 shows that the microwave power peaks for an applied field of 5 kG when the field is varied from 0 to 20 kG. Similar behavior is observed in computer calculations. We believe that when the magnetic field is weak (but strong enough to guide the beam through the slot) the consequent high beam divergence leads to reduced output power. For a strong magnetic field, the reflected electrons are so tightly bound to the field lines that they reenter the diode, leading to reduced power output. Thus at the intermediate value of the magnetic field (about 5 kG, in our experiment) the power reaches a maximum. When microwave power is substantial with the thick anode, we observe insignificant power with a thin anode substituted for the thick anode. This implies that under the same conditions, the radiation mechanism with the thick anode is much more efficient than with the thin anode. This is likely the result of the thick anode intercepting reflected electrons. Also, after many shots the anode is discolored at the slot edge on the output waveguide side, suggesting electron impact.

We performed computer simulations to model the standard case (B_z =9.3 kG, gap =3.7 cm) to examine the electron being reflected into the diode region. We chose computer modeling since the highly nonlinear and time-dependent behavior of this system probably precludes accurate analytic modeling. The $2\frac{1}{2}$-dimensional, fully electromagnetic, relativistic, particle-in-cell code ISIS was used with axisymmetric cylindrical geometry. A Monte Carlo transport technique was used in the code to calculate electron trajectories in the anode material.[15]

Figure 4 shows the calculated particle plots in the r-z and the p_z-z planes for a typical time. Here r and z are the usual cylindrical coordinates, and p_z is the axial-relativistic-electron momentum. The particle trajectories in the r-z plane show the beam flowing from the cathode to the anode through the annular slot. The beam radius decreases slightly as it is guided through the collimator. This pinching, observed experimentally in x-ray pinhole photographs of the anode, results from the anode's short-

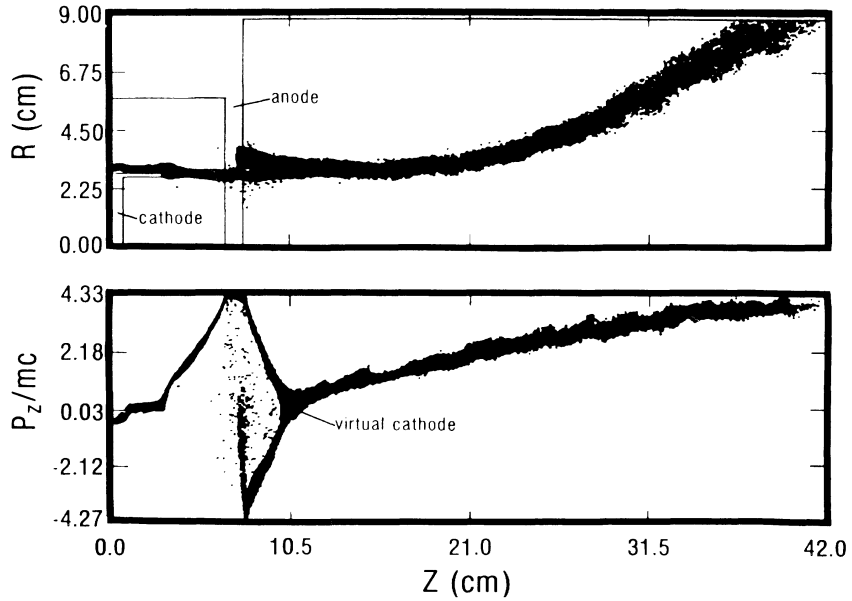

FIG. 4. Particle plots from computer simulation for B =9.3 kG and 3.7-cm anode-cathode gap. The top graph shows electrons in the r-z plane; the bottom graph shows electrons in the (p_z/mc)-z plane.

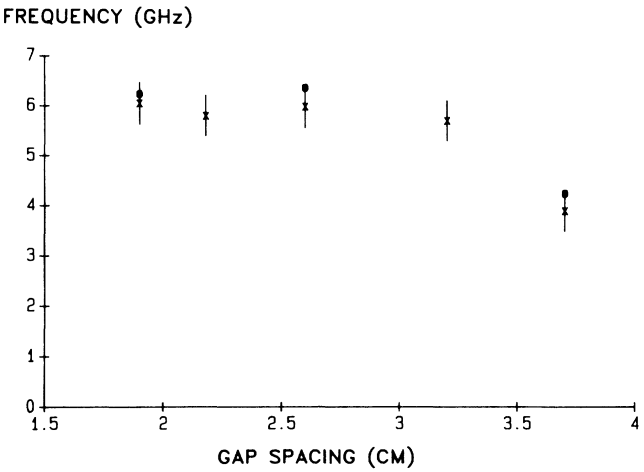

FIG. 5. Dominant frequency vs anode-cathode gap spacing for $B=9.3$ kG. The crosses with error bars are the measured values and the circles are values of the injected relativistic beam plasma frequency obtained from computer simulations.

ing of the electron beam's radial electric field. Downstream of the anode, the transmitted beam electrons flow along the flaring magnetic field lines at the magnetic field coil end and strike the waveguide. The reflected component strikes the collimator. In this case, the reflected beam is prevented from reentering the diode primarily because the reflected beam radius increases. Estimates of the radial forces acting on the beam show the applied magnetic field is weak enough for this to occur. The phase-space plot shows that the virtual cathode forms 2.2 cm from the downstream side of the anode. Here one can see that most of the reflected electrons (that is, those with negative momentum) strike the waveguide side of the anode and are absorbed. Very few electrons flow back into the diode region. Thus microwave power scaling with magnetic field, power measurements with and without the thick anode, anode discoloration, and computer simulations demonstrate that we have achieved the desired nonreflecting operation.

We performed frequency scaling experiments to ensure that virtual-cathode oscillations produced the radiation. Since the microwaves are generated by virtual-cathode oscillations, we expected the radiation frequency to scale with the relativistic beam plasma frequency. One-dimensional computer calculations support this conjecture. Figure 5 shows the measured dominant frequency as a function of anode-to-cathode separation for an applied magnetic field of 9.3 kG. Also shown are values of the relativistic beam plasma frequency for the electron beam obtained from computer simulations of the diode region. The agreement is quite close, indicating that virtual-cathode oscillations produce the radiation. We also investigated the scaling of the dominant frequency as a function of applied magnetic field strength for 2.6-cm anode-cathode gap. Here the frequency was expected to change primarily as a result of beam thickness variations. The frequency was only weakly dependent on the magnetic field. This rules out processes that depend strongly on magnetic field such as gyrotron emission.

Power measurements were made for the standard case ($B_z=9.3$ kG, gap $=3.7$ cm). We measured the power-density distribution and found that TM_{02} was the dominant waveguide mode. The inferred peak power level was 1.4 ± 0.3 GW at the dominant frequency of 3.9 ±0.4 GHz with several hundred megawatts emitted in harmonic radiation. The dominant calculated waveguide mode was TM_{02}, and the calculated frequency was 3.6 GHz, both in good agreement with observations. Computed power levels were somewhat lower than the measured values.

The authors acknowledge the expert assistance of Gary Ashel, Herbert Harry, Paul Roybal, Roberta Showalter, and Robert Wheat, and also acknowledge many stimulating discussions with L. E. Thode. This work was supported by the U. S. Strategic Defense Initiative Office of Innovative Science and Technology and managed by Harry Diamond Laboratories, and by the U. S. Department of Energy.

[1]R. B. Miller, *Introduction to the Physics of Charged Particle Beams* (Plenum, New York, 1982), p. 213.

[2]R. A. Mahaffey, P. Sprangle, J. Golden, and C. A. Kapetanakos, Phys. Rev. Lett. **39**, 843 (1977).

[3]H. E. Brandt, A. Bromborsky, H. B. Bruns, and R. A. Kehs, in *Proceedings of the Second International Topical Conference on High Power Electron and Ion Beam Research and Technology, Ithaca, NY, 1977,* edited by J. A. Nation and R. N. Sudan (Cornell Univ. Press, Ithaca, NY, 1977).

[4]J. M. Buzzi, H. J. Doucet, B. Etlicher, P. Haldenwang, A. Huetz, H. Lamain, C. Rouillé, J. Cabé, J. Delvaux, J. C. Jouys, and C. Peugnet, in Ref. 3, p.663.

[5]A. N. Didenko, A. G. Zherlitsyn, A. S. Sulakshin, G. P. Formenko, V. I. Tsvetkov, and Yu.G Shtein, Pis'ma Zh. Tekh. Fiz. **9**, 1510 (1983) [Sov. Tech. Phys. Lett. **9**, 647 (1983)].

[6]D. J. Sullivan, IEEE Trans. Nucl. Sci. **30**, 3426 (1983).

[7]T. J. T. Kwan and L. E. Thode, Phys. Fluids **27**, 1570 (1984).

[8]H. A. Davis, R. R. Bartsch, L. E. Thode, E. G. Sherwood, and R. M. Stringfield, Phys. Rev. Lett. **55**, 2293 (1985).

[9]H. Sze, J. Benford, T. Young, D. Bromley, and B. Harteneck, IEEE Trans. Plasma Sci. **13**, 492 (1985).

[10]R. D. Scarpetti and S. C. Burkhardt, in Ref. 9, p. 506.

[11]C. Clark, private communication.

[12]T. J. T. Kwan and L. E. Thode, Bull. Am. Phys. Soc. **27**, 1017 (1982).

[13]T. J. T. Kwan, Phys. Rev. Lett. **57**, 1895 (1986).

[14]L. E. Thode, B. B. Godfrey, and W. R. Shanahan, Phys. Fluids **22**, 747 (1979).

[15]T. J. T. Kwan and C. M. Snell, in *Monte-Carlo Methods and Applications in Neutronics, Photonics, and Statistical Physics,* edited by R. Alcouffe, R. Dautray, A. Forster, G. Ledanois, and B. Mercier (Springer-Verlag, Berlin, 1985).